Applied Catalysis B: Environmental 196 (2016) 185–192

Contents lists available at ScienceDirect

Applied Catalysis B: Environmental

journal homepage: www.elsevier.com/locate/apcatb

Synthesis of rhodium-platinum bimetallic catalysts supported on SBA-15 by chemical fluid deposition for the hydrogenation of terephthalic acid in water

Wen Yu, Yen-Ping Hsu, Chung-Sung Tan *

Department of Chemical Engineering, National Tsing Hua University, Hsinchu 30013, Taiwan, ROC

ARTICLE INFO

Article history:
Received 6 March 2016
Received in revised form 30 April 2016
Accepted 17 May 2016
Available online 18 May 2016

Keywords:
Bimetallic catalyst
Rh-Pt
Chemical fluid deposition
Hydrogenation in water
TPA

ABSTRACT

In this study, rhodium-platinum bimetallic catalysts supported on mesoporous silica SBA-15 (Rh-Pt/SBA-15) were synthesized by a chemical fluid deposition (CFD) method using supercritical CO_2 as a solvent. Uniformly dispersed Rh-Pt nanoparticles with an average size (~6.1 nm) smaller than the pore size of SBA-15 were obtained. The performance of the prepared catalysts in the hydrogenation of terephthalic acid (TPA) in water was investigated in spite of the poor solubility of TPA in water. The Rh-Pt/SBA-15 bimetallic catalyst synthesized at a 70:30 weight ratio of Rh to Pt ($Rh_{70}Pt_{30}$/SBA-15) exhibited a better catalytic activity than its monometallic counterparts (Rh/SBA-15 and Pt/SBA-15). A TPA conversion as high as 74.3% was achieved using the $Rh_{70}Pt_{30}$/SBA-15 bimetallic catalyst at 80 °C and 5 MPa of H_2 in a 2-h reaction, whereas the conversion of TPA over the Rh/SBA-15 catalyst was found to be 24.2%, and no reaction was observed in the presence of Pt/SBA-15 catalyst. The enhanced activity of the Rh-Pt/SBA-15 catalyst was attributed to the synergistic effect of Rh and Pt in the bimetallic alloy. In the Rh-Pt/SBA-15 bimetallic catalysts, it is believed that Pt helped the adsorption of arenes on the active sites and Rh played a key role in the catalytic hydrogenation of TPA. Moreover, a complete conversion of TPA could be achieved at 80 °C and 5 MPa of H_2 by increasing the reaction time to 4 h.

1. Introduction

Terephthalic acid (TPA) is an important raw material that is widely used in the polyester industry, particularly for the synthesis of polyethylene terephthalate (PET). However, the polyesters that are synthesized directly from TPA are non-biodegradable due to the presence of benzene rings in the structure. Considering the environmental impact of plastic pollution, many processes have been developed to synthesize biodegradable polyesters [1,2], but the process that uses the hydrogenated product of TPA, i.e., 1,4-cyclohexanedicarboxylic acid (1,4-CHDA) [3–6], as raw material is the most attractive synthesis process. Several multi-step processes have been reported for preparing 1,4-CHDA, in which the benzene rings are hydrogenated under an acidic environment after converting TPA into esters or metal salts of TPA [7]. The direct hydrogenation of TPA is obviously a more economical and promising approach compared with other multi-step processes [6]; however, there are a number of challenges hindering its commercialization. One major problem in the hydrogenation of organic compounds containing benzene rings is that it is generally performed under severe conditions, i.e., at high temperature, as in the case of hydrogenation of TPA. The choice of solvent for hydrogenation reactions is another critical issue. Water is one of the most attractive green solvents because it is nontoxic, nonflammable and readily available. However, the limited solubility of TPA in water (0.25 g/100 ml at 150 °C and 1.7 g/100 ml at 200 °C) hinders the commercial use of water as a solvent [4,8]. Therefore, the proper selection of optimal solvent and highly active catalysts is important to catalyze the hydrogenation of benzene rings under mild conditions.

Over the past decade, several research groups have made significant efforts to synthesize effective catalysts for the hydrogenation of TPA in water. Sumner and Gustafson et al. [9] performed the catalytic hydrogenation of TPA in water over a palladium catalyst (Pd/C) at 195–230 °C, resulting in a 98.4% yield for 1,4-CHDA. Kayou and Nanba [10] also used a Pd/C catalyst for the hydrogenation of TPA in water, in which the TPA conversion and 1,4-CHDA yield were found to be 99.2% and 95.4%, respectively, in 1 h at 150 °C and 3 MPa of H_2. However, the high cost of the precious metal (Pd) limited its industrial applications. Some patents have proposed the

* Corresponding author.
E-mail address: cstan@mx.nthu.edu.tw (C.-S. Tan).

http://dx.doi.org/10.1016/j.apcatb.2016.05.034
0926-3373/

use of catalysts containing relatively cheaper noble metals as the active components and active carbon as the support such as Ru/C for this reaction. However, the results showed that the Ru/C catalyst had a poor catalytic activity and selectivity [4]. Zhu et al. [11] used a Ru/Al_2O_3 catalyst for the hydrogenation of TPA and the highest conversion of TPA was found to be 95.4% at 140 °C, 5.0 MPa of H_2 in 1.5 h. All of the aforementioned reactions performed at high temperatures due to the limited solubility of TPA in water are certainly less favorable based on their energy consumption and processing costs. Thus, more effective catalysts need to be developed for the hydrogenation of TPA under mild conditions in water.

The preparation of metal catalysts using chemical fluid deposition (CFD) has received considerable attention in recent years [12–15]. CFD has been widely used in the preparation of supported metal catalysts because it fully exploits the desirable attributes of supercritical fluids to deposit metals within a nanoporous matrix, including its gas-like transport properties, liquid-like dissolving power, near-zero surface tension and gas-like viscosity, which could avoid the collapse of the ordered pores of the support during drying. Supercritical CO_2 ($scCO_2$) is the most commonly used green solvent in CFD because it is readily available, inexpensive, nontoxic, and nonflammable and has a moderate critical temperature and pressure (31.7 °C and 7.38 MPa) [16–20]. Many hydrogenation catalysts have been synthesized over the last decade by CFD using $scCO_2$ as a solvent such as Ag/MCM-41 [21], Ru/MOF nanocomposites [22], Ru/MCM-41 [15] and Ru-Rh, Ru-Pd and Rh-Pd bimetallic nanoparticles deposited on mesoporous silica MCM-41 [14]. However, the active components of most of these catalysts included precious noble metals such as Ru, Rh and Pd, thus making them less attractive for industrial use. As a result, many bimetallic catalysts containing cheaper noble or transition metals such as Fe [23–25], Ni [26–28], and Pt [29–31] have been developed. More importantly, the catalytic performance of the bimetallic catalysts can be improved compared with that of the monometallic catalysts due to the anchoring or synergistic effect of bimetallic nanoparticles in the catalysts [29,32,33]. Abu Bakar et al. [33] reported that the Ni-Pt/MCM-41 bimetallic catalyst exhibited a higher catalytic activity than did the monometallic Pt/MCM-41 catalyst due to the anchoring effect of non-reduced Ni^{2+} ions, which resulted in well-dispersed Pt particles. Pan and Wai [29] demonstrated that the Rh-Pt nanoparticles deposited on multi-walled carbon nanotubes (MWNTs) using a one-step sonochemical method exhibited a strong synergistic effect compared with the individual Pt or Rh nanoparticles for the catalytic hydrogenation of polycyclic aromatic hydrocarbons. Although MWNT-supported metal nanoparticles exhibited the highest catalytic activity in hydrogenation of aromatic compounds compared with those of the other supported metal catalysts in the order MWNTs > SiO_2-Al_2O_3 > ZrPSi [34], the hydrophobic nature of MWNTs would not be favorable for hydrogenation in water. Therefore, choosing a hydrophilic support is of great importance for the uniform dispersion of catalyst in water. Ordered mesoporous silica materials, particularly SBA-15, is thus a promising catalyst support material for hydrogenation reactions because it is hydrophilic and exhibits larger pores, thicker walls and higher hydrothermal stability compared with other types of mesoporous silica materials [35]. However, to the best of our knowledge, neither the synthesis of Rh-Pt bimetallic catalysts supported on SBA-15 using CFD nor their performance for the hydrogenation of TPA in water under mild conditions has been reported in the open literature so far.

Here, the synthesis of Rh-Pt/SBA-15 bimetallic catalyst by CFD using $scCO_2$ as a solvent, rhodium(III) acetylacetonate and platinum(II) acetylacetonate as the metal precursors, and SBA-15 as a support has been reported. The performance of the prepared catalysts was tested in the hydrogenation of TPA in water. Moreover, the hydrogenation of other important aromatic compounds in water was investigated. An effective Rh-Pt/SBA-15 bimetallic catalyst for the hydrogenation of TPA in water under mild conditions was synthesized by CFD in this study. The results indicate that the direct hydrogenation of aromatic compounds for producing biodegradable polyesters is possible using a more effective bimetallic catalyst.

2. Experimental

2.1. Materials

Rhodium(III) acetylacetonate $Rh(acac)_3$ (purity > 99.9%) and Platinum(II) acetylacetonatenate $Pt(acac)_2$ (purity > 98.0%) were purchased from Strem Chemicals Inc., and were all used as received. CO_2 (purity > 99.9%) and H_2 (purity > 99.9%) were purchased from Linde LienHwa Industrial Gases. Terephthalic acid (purity > 98.0%), bisphenol A (purity ≥ 99.0%), benzoic acid (purity > 99.5%), isophthalic acid (purity > 99.0%), tetrahydrofuran (THF, purity ≥ 99.9%) and dimethyl phthalate (purity > 99.0%) were purchased from Sigma-Aldrich and were all used as received. Dimethyl sulfoxide-d_6 (purity ≥ 99.9%) was purchased from Sigma-Aldrich. The hexagonal mesoporous silica SBA-15 was synthesized using the hydrothermal technique [36], with an average pore size of 6.7 nm, a surface area of 1030 m^2/g and a pore volume of 1.06 cm^3/g.

2.2. Catalyst preparation

Metal beta-diketonate compounds, $Rh(acac)_3$ and $Pt(acac)_2$, were used as the metal precursors in this study. Because the solubilities of $Rh(acac)_3$ and $Pt(acac)_2$ in $scCO_2$ are not high enough to achieve the desired theoretical metal loading of 5.6 wt%, THF was therefore used to impregnate more precursors into the support SBA-15 first based on the fact that the solubilities of $Rh(acac)_3$ and $Pt(acac)_2$ in THF are much higher than those in $scCO_2$ [14,37]. As pointed out by Yen et al. [14] and Dhepe et al. [30], applying supercritical fluid treatment after the removal of organic liquid such as THF, which is after impregnation, can obtain a high dispersion of precursor inside the mesoporous channels. In a consequence, uniform dispersion of nano catalyst particles inside the pores of the support after the reduction by hydrogen can therefore be obtained. Thus, in the current study, $scCO_2$ treatment was also applied to re-disperse precursors inside the pores of the support after the removal of THF. In typical trials, the precursors and SBA-15 were mixed with a desired weight ratio of metal. THF was then added to dissolve the metal precursors and ultra-sonicating was used to accelerate the impregnation process. After uniform mixing, THF was removed using a rotary vacuum evaporator. The remaining sample powders were then transferred into a high pressure stainless steel reactor placed in an oven and subjected to a $scCO_2$ treatment. The $scCO_2$ treatment was performed at 40 °C and 17.24 MPa for 2 h under stirring. After releasing CO_2, the $scCO_2$ treated catalysts were reduced under a flow of H_2 (20 ml/min) at 400 °C for 2 h.

2.3. Catalyst characterization

2.3.1. Transmission electron microscopy (TEM) and high resolution transmission electron microscopy (HRTEM)

The images of TEM were taken by Joel JEM-2100 at an accelerating voltage of 200 kV. The synthesized catalyst powders were diluted with ethanol and then under ultra-sonication for 5 min. Droplets of the prepared sample were put on a copper grid and dried in a vacuum oven of 100 °C overnight. The particle size distribution was determined by using the imaging analysis software OPTIMAS5. At least 300 particles were recorded in order to obtain the average particle size and standard deviation. The microstruc-

ture of the sample was obtained with a high resolution transmission electron microscopy (JEOL JEM-2100F).

2.3.2. Energy dispersive X-ray spectroscopy (EDS)

EDS was conducted on Oxford 6587 coupled with a scanning electron microscope (HITACHI SU 8010 SEM). The analysis of the metal content in the nanocatalyst was taken for at least 5 samples to obtain the average value with a standard deviation within 8%.

2.3.3. Powder X-ray diffraction (XRD)

XRD was conducted on a Rigaku Ultima IV Powder X-ray Diffractometer with Cu-Kα radiation at 40 kV, 20 mA. The scan rate was 0.2°/min starting at 10° to 90° (2θ).

2.3.4. X-ray photoelectric spectroscope (XPS)

XPS was conducted on High resolution X-ray Photoelectron Spectrometer Electron (ULVAC-PHI XPS, PHI Quantera) with 180° Spherical Capacitor Analyzer + 32 Channel Detector. Monochromatic radiation from an Al anode X-ray source was used for excitation. The vacuum degree was at a base pressure lower than 5×10^{-5} torr during the measurement.

2.3.5. Hydrogenation of TPA and other aromatic compounds

Catalytic reactions were performed in a 300 ml stainless steel high-pressure reactor (Parr Instruments Company) equipped with a pressure gauge, a temperature controller and an agitator. In a typical hydrogenation experiment, 0.3 g of TPA, 0.0250 g of catalyst and 50 g of deionized water were mixed together and charged into the reactor. The agitator speed was set to 1000 rpm, and the reaction temperature was kept constant at 80 °C. Hydrogen was introduced into the reactor to initiate the hydrogenation at a desired pressure (5 MPa) for a given reaction time. After cooling to room temperature, the reaction system was depressurized, and water was removed by evaporation. The final products were diluted with dimethyl sulfoxide-d_6 and then analyzed by gas chromatography (Agilent 6890N fitted with a HP-5MS capillary column and a FID detector). The conversion of TPA was defined as the moles of TPA converted with respect to the total moles of TPA in the feed. The ratios of *trans*-1,4-CHDA and *cis*-1,4-CHDA were determined by ^{1}H NMR (500 MHz, DMSO, Varian Unity Inova, 500 NMR).

3. Results and discussion

3.1. Characterization of the mesoporous silica SBA-15-supported nanocatalysts

A series of Rh, Pt monometallic and Rh-Pt bimetallic catalysts supported on SBA-15 with different weight ratios of Rh to Pt were synthesized by CFD using $scCO_2$ as a solvent. In this study, the catalysts were named based on the initial weight ratio of Rh to Pt (for example, $Rh_{70}Pt_{30}$/SBA-15 represented a 70:30 weight ratio of Rh to Pt).

The TEM images of the prepared catalysts (Fig. 1) revealed a fine dispersion of nanoparticles inside the pores of SBA-15, indicating that the metal precursor dissolved in $scCO_2$ could effectively diffuse into the pores of SBA-15 and deposit onto the walls of channels after depressurization without destroying the hexagonal pore structure due to the near-zero surface tension of $scCO_2$. The average sizes with the standard deviation obtained from the TEM images of different metallic nanoparticles were as follows: 11.2 ± 4.3 nm for Pt/SBA-15, 7.2 ± 3.3 nm for Rh/SBA-15, 7.6 ± 2.6 nm for $Rh_{41}Pt_{59}$/SBA-15, 6.6 ± 2.0 nm for $Rh_{50}Pt_{50}$/SBA-15, 6.1 ± 1.9 nm for $Rh_{70}Pt_{30}$/SBA-15, and 5.9 ± 1.8 nm for $Rh_{81}Pt_{19}$/SBA-15. The large average size of Pt nanoparticles in the Pt/SBA-15 catalyst was attributed to the aggregation of metal nanoparticles that were mainly deposited outside the pores (large black particles seen in Fig. 1a) during the high-temperature reduction process. Compared with the Pt nanoparticles, the Rh nanoparticles in the monometallic catalyst were smaller and exhibited better dispersion in the support. In the case of Rh-Pt/SBA-15 bimetallic catalysts, the better dispersion of Rh was beneficial to stabilize the dispersion of Pt in the support, which further helped form smaller Pt nanoparticles than those observed in the Pt/SBA-15 catalyst.

The high resolution TEM image (Fig. 1g) showed that the metal particles were inside the pores of the support. The lattice fringes of the metal particles indicated the highly crystalline nature of particles. The lattice fringe with D-spacing of 0.22 nm belonged to both the (111) lattice planes of Rh and Pt, which was in good agreement with the XRD results. The elemental mapping images shown in Fig. 1h confirmed the coexistence of Rh and Pt in the metal particles in the catalyst, giving further evidence for the formation of Rh-Pt bimetallic catalyst.

Fig. 2 presents the XRD patterns of the catalyst samples. The XRD pattern of the Pt/SBA-15 catalyst (Fig. 2a) showed four diffrac-

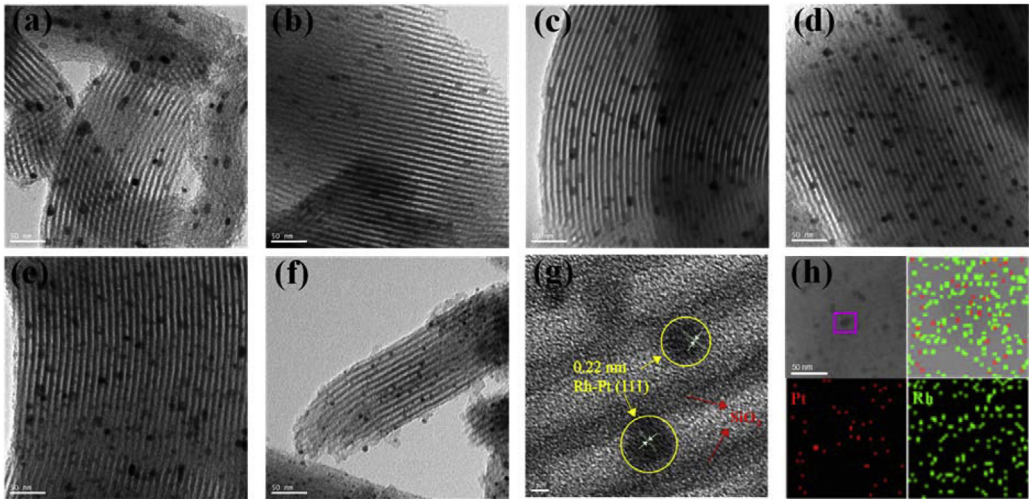

Fig. 1. TEM images of Rh-Pt/SBA-15 bimetallic catalysts synthesized at 40 °C and 17.24 MPa in 2 h at different Rh to Pt ratios: (a) Pt/SBA-15, (b) Rh/SBA-15, (c) $Rh_{41}Pt_{59}$/SBA-15, (d) $Rh_{50}Pt_{50}$/SBA-15, (e) $Rh_{70}Pt_{30}$/SBA-15 and (f) $Rh_{81}Pt_{19}$/SBA-15; (g) HRTEM image of the Rh-Pt particles in $Rh_{70}Pt_{30}$/SBA-15; (h) The elemental mapping images of Rh and Pt for the particle in the $Rh_{70}Pt_{30}$/SBA-15 bimetallic catalyst.

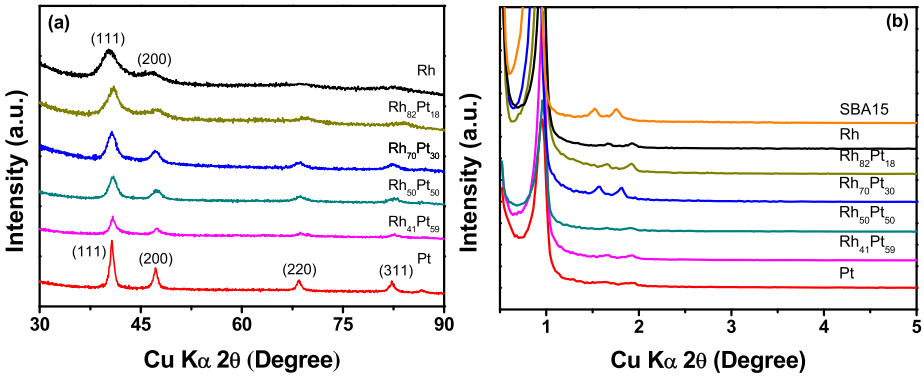

Fig. 2. (a) Powder wide-angle XRD patterns and (b) small-angle XRD patterns of the prepared catalysts.

tion peaks at 2θ = 40.6°, 46.9°, 68.6° and 82.4°, which represented the (111), (200), (220), and (311) planes, respectively, indicating the face-centered cubic structure of Pt nanoparticles (JCPDS Card No. 87-0647). A representative XRD pattern of the Rh/SBA-15 catalyst showed only two reflections at 41.3° and 47.7°, which corresponded to the (111) and (200) planes of the face-centered cubic Rh nanoparticles (JCPDS card No. 87-0714). The XRD patterns of the Rh-Pt/SBA-15 bimetallic catalysts showed four diffraction peaks at 40.8°, 47.2°, 68.4°, and 82.6° (Fig. 2a), corresponding to the (111), (200), (220), and (311) planes, which were similar to the XRD results reported by Pan and Wai [29], indicating the formation of Rh-Pt alloy. The diffraction peak corresponding to the (111) plane of each bimetallic catalyst was higher than the diffraction peak corresponding to the (200) plane, which might have been due to the random orientation of SBA-15 [38,39]. In addition, the average particle sizes of Rh, Pt, and Rh-Pt nanoparticles were estimated from the diffraction peaks corresponding to the (111) [40], (220) [41], and (220) [42] planes, respectively, using the Scherrer's formula,

$$\tau = \frac{K\lambda}{\beta \cos\theta} \quad (1)$$

where τ is the average particle size, K = 0.9, λ is the wavelength of X-ray radiation (Cu Kα source, 0.154056 nm), β is the full width at half maximum of the diffraction peak in radians, and θ is the diffraction angle of the peak. The average sizes of the Rh, Pt, and Rh-Pt nanoparticles calculated using Eq. (1) were as follows: Pt/SBA-15 (12.80 nm), Rh/SBA-15 (4.61 nm), $Rh_{41}Pt_{59}$/SBA-15 (6.83 nm), $Rh_{50}Pt_{50}$/SBA-15 (6.33 nm), $Rh_{70}Pt_{30}$/SBA-15 (5.56 nm), and $Rh_{81}Pt_{19}$/SBA-15 (6.64 nm), which were consistent with the results obtained from TEM analysis. Moreover, the small-angle XRD pattern (Fig. 2b) displayed three characteristic diffraction peaks corresponding to the (100), (110), and (200) planes of SBA-15. This result confirmed that the synthesis of supported metal catalysts by the CFD method could avoid the structural collapse of the mesoporous support, as seen from the TEM images (Fig. 1).

EDS measurements can reveal the elemental distribution of the catalysts. The metal loading results for the prepared catalysts using EDS are shown in Table 1. Except for the Pt/SBA-15 catalyst, the metal loadings of the other catalysts were approximately 70% of the theoretical limit. The lowest metal loading of the Pt/SBA-15 catalyst was probably due to the lower solubility of $Pt(acac)_2$ in $scCO_2$ than that of $Rh(acac)_3$ [43]. Since high utilization of noble metal is of great importance in the preparation of industrial catalysts, several techniques have been proposed to prepare catalyst with high utilization of noble metal, including the use of precursors with high solubility in $scCO_2$ such as cycle metal precursors [15] or modified supports that could provide more sites for metal adsorption and

Table 1
Results of the metal loading of the prepared catalysts analyzed by EDS.

Catalyst[a]	Metal loading (wt%)	Rh loading (wt%)	Pt loading (wt%)
Rh/SBA-15[b]	2.0	2.0	n/a
Rh/SBA-15	4.0	4.0	n/a
$Rh_{82}Pt_{18}$/SBA-15	4.1	2.9	1.2
$Rh_{70}Pt_{30}$/SBA-15	3.8	2.1	1.7
$Rh_{50}Pt_{50}$/SBA-15	4.0	1.4	2.6
$Rh_{41}Pt_{59}$/SBA-15	3.8	1.0	2.8
Pt/SBA-15	3.5	n/a	3.5
$Rh_{68}Pt_{32}$/SBA-15	3.7	2.0	1.7

[a] The theoretical metal loading was 5.6 wt%.
[b] The theoretical metal loading was 2.8 wt%.

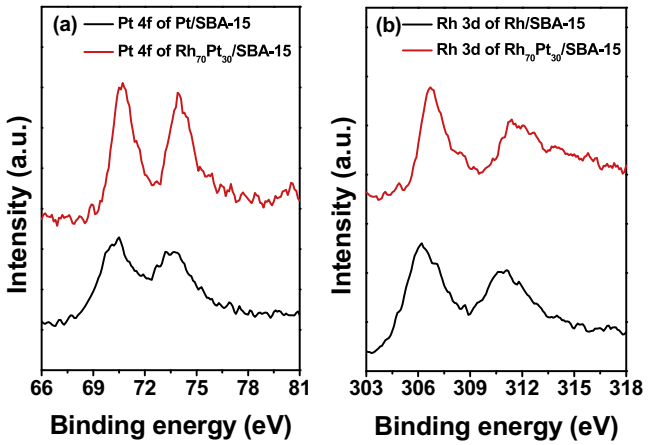

Fig. 3. XPS spectra of Pt/SBA-15, Rh/SBA-15 and $Rh_{70}Pt_{30}$/SBA-15.

stabilization such as SBA-15 coated with carbon nitrile [44,45]. Nevertheless, the method used in this study has been widely applied to disperse catalyst uniformly inside the pores of the support without surface modification.

The XPS analysis was performed on the monometallic and bimetallic catalysts synthesized by CFD. The Pt/SBA-15 catalyst showed two peaks in the Pt 4f spectrum at binding energies of 70.4 and 73.3 eV, which were consistent with the zero-valence state of Pt metal species for the Pt ($4f_{7/2}$) and Pt ($4f_{5/2}$) core levels [46], respectively. The Rh/SBA-15 catalyst exhibited two peaks in the Rh 3d spectrum at binding energies of 306.1 eV for the Rh ($3d_{5/2}$) and 310.7 eV for the Rh ($3d_{3/2}$) core levels of Rh^0 species. The XPS spectra of the $Rh_{70}Pt_{30}$/SBA-15 bimetallic catalyst are shown in Fig. 3. The binding energies of two Pt 4f peaks for the $Rh_{70}Pt_{30}$/SBA-15 bimetallic catalyst were 70.8 and 74 eV for the Pt ($4f_{7/2}$) and ($4f_{5/2}$) core levels, respectively (Fig. 3a). The binding energies of

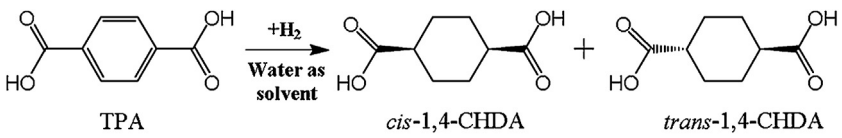

Fig. 4. The scheme for hydrogenation of TPA in water.

two Rh 3d peaks for the $Rh_{70}Pt_{30}$/SBA-15 bimetallic catalyst were 306.6 and 311.5 eV for the Rh ($3d_{5/2}$) and ($3d_{3/2}$) core levels, respectively (Fig. 3b). A shoulder peak appeared for the $Rh_{70}Pt_{30}$/SBA-15 bimetallic catalyst at 314.0 eV (Fig. 3b), corresponding to the binding energy of Rh^0 species for the Rh ($4d_{5/2}$) core level. A difference in the Rh 3d binding energies was observed between the Rh/SBA-15 and $Rh_{70}Pt_{30}$/SBA-15 catalysts. It was speculated that the formation of Rh-Pt alloy could lead to these Rh 3d binding energy shifts.

3.2. Hydrogenation of TPA in water

In this study, the prepared monometallic (Pt/SBA-15 and Rh/SBA-15) and bimetallic (Rh-Pt/SBA-15) catalysts were tested in the hydrogenation of TPA in water (Fig. 4), and the obtained results are shown in Table 2. The conversion of TPA was only 24.2% using the Rh/SBA-15 catalyst at 80 °C and 5 MPa of H_2 in 2 h, whereas no reaction was observed in the presence of Pt/SBA-15 catalyst. These results showed that the Rh/SBA-15 catalyst had a poor catalytic activity for the hydrogenation of TPA, but the Pt/SBA-15 catalyst exhibited no catalytic activity for the hydrogenation reaction. This poor catalytic performance of Rh/SBA-15 and Pt/SBA-15 might be attributed to the larger particle sizes of Rh and Pt in SBA-15 that reduced the active sites for the reaction and the adsorption capacity of reactant [47,48], thus resulting in a lower conversion of TPA. However, the conversion of TPA increased significantly using the Rh-Pt/SBA-15 bimetallic catalyst. The highest conversion in a 2-h reaction was found to be 74.3% using the $Rh_{70}Pt_{30}$/SBA-15 catalyst, which was considerably higher than that using the Rh/SBA-15 catalyst. Moreover, a complete conversion of TPA could be achieved using the $Rh_{70}Pt_{30}$/SBA-15 catalyst by increasing the reaction time to 4 h at 80 °C. One possible reason for the complete conversion of TPA under this mild condition could be the "on water" reaction [49]. The strong H-bonding interaction between the SBA-15 support and water could account for the on water effect observed in this reaction under mild conditions. In addition, the enhanced activity of the $Rh_{70}Pt_{30}$/SBA-15 bimetallic catalyst compared with that of their monometallic counterparts (Rh/SBA-15 or Pt/SBA-15) could be attributed to the following two factors: (i) the strong synergistic effect of Rh and Pt in the bimetallic alloy for hydrogenation of alkylbenzenes, i.e., the benzene rings could be easily adsorbed in a bridge configuration on Pt (111) during the catalytic hydrogenation process [29], (ii) the weak hydrogen binding energy that could facilitate H_2 activation on the surface of the alloy catalyst [50,51]. Thus, according to the proposed reaction mechanism for the Rh-Pt bimetallic catalyst, Pt helped the adsorption of TPA on the active sites, whereas Rh played a key role in the hydrogenation of TPA.

As compared with the monometallic catalyst Pt/SBA-15, the catalytic activity of the prepared bimetallic catalysts increased with increasing Rh content and followed the order $Rh_{70}Pt_{30}$/SBA–15 > $Rh_{50}Pt_{50}$/SBA–15 > $Rh_{41}Pt_{59}$/SBA–15 > Pt/SBA-15. This trend can be explained by the addition of more active catalyst Rh and the increase of the synergistic effect between the two metals. But this trend was not monotonic. The catalytic activity was observed to decrease with further increase of Rh/Pt ratio, i.e., $Rh_{70}Pt_{30}$/SBA–15 > $Rh_{82}Pt_{18}$/SBA–15 > Rh/SBA-15, even though more activate catalyst Rh increased. These results demonstrated that the choice of a bimetallic catalyst with a proper Rh/Pt ratio is essential for hydrogenation reaction.

In addition, the conversion of TPA using the $Rh_{70}Pt_{30}$/SBA-15 catalyst synthesized by CFD was higher than that obtained using the $Rh_{68}Pt_{32}$/SBA-15 catalyst synthesized by simple mechanical mixing. The specific activity, defined as moles reacted per mole of metal in the catalyst per unit time [29,52], was used to compare the catalytic activities of metals in the prepared catalysts. As shown in Table 2, the specific activity value for hydrogenation of TPA by $Rh_{70}Pt_{30}$/SBA-15 synthesized by CFD was found to be 280.2 h^{-1}, which was approximately nine times higher than the $Rh_{68}Pt_{32}$/SBA-15 catalyst synthesized via mechanical mixing (20.9 h^{-1}). This result indicated that the synergy between Rh and Pt was because of the ensemble effect and not just the mixing effect, which in turn proved that this synergistic effect was the main reason for the enhanced activity of the bimetallic catalysts synthesized by CFD.

A complete conversion of TPA in water was observed under the following reaction conditions: 0.0250 g $Rh_{70}Pt_{30}$/SBA-15, 0.3 g TPA, 50 g water, 5 MPa H_2, 80 °C, and 4 h, whereas no conversion of TPA was observed in methanol under the same reaction conditions in spite of its higher solubility in methanol [53] by approximately an order of magnitude compared with that in water. These conversion results indicated that the hydroxyl groups on the silica surface

Table 2
The hydrogenation of TPA over the prepared monometallic and bimetallic catalysts.

Catalyst[a]	Reaction time (h)	Solvent	Conversion (%)	*trans*:*cis*	Specific activity (h^{-1})
Rh[b]	2	Water	11.4	36:64	64.8
Rh	2	Water	24.2	70:30	67.8
$Rh_{82}Pt_{18}$	2	Water	62.7	61:39	196.7
$Rh_{70}Pt_{30}$	2	Water	74.3	60:40	280.2
	4	Water	99.6	64:36	187.8
	4	Methanol	0	n/a	n/a
$Rh_{50}Pt_{50}$	2	Water	37.8	83:17	152.1
$Rh_{41}Pt_{59}$	2	Water	9.1	59:41	40.8
Pt	4	Water	<1	n/a	n/a
$Rh_{68}Pt_{32}$[c]	2	Water	5.4	40:60	20.9

[a] Catalysts synthesized by CFD method, 0.0250 g, the theoretical metal loading was 5.6 wt%.
[b] Catalysts synthesized by CFD method, 0.0250 g, the theoretical metal loading was 2.8 wt%.
[c] Catalysts synthesized by mechanical mixing 0.0125 g Pt/SBA-15 and 0.0125 g Rh/SBA-15, the theoretical metal loadings of Pt/SBA-15 and Rh/SBA-15 were both 2.8 wt%.

could form hydrogen bonds with water molecules [54], which could further help the water molecules surround the catalyst and improve its dispersion in the reaction system. It can be seen from Table 2 that the specific activity values were significantly higher for the bimetallic catalysts than for the monometallic catalysts, which also indicated a synergistic relationship between Rh and Pt (formed by either metal–metal bonding or changing the dispersion of available active sites on the catalyst surface). Therefore, the $Rh_{70}Pt_{30}$/SBA-15 bimetallic catalyst synthesized by CFD was found to be an effective catalyst for the hydrogenation of TPA in water under mild conditions.

Further, 1,4-CHDA obtained by hydrogenation of TPA was a mixture of the *cis*- and *trans*-form. Considering the demand for the hydrogenated polyester with excellent heat resistance, the *trans*-form possessing better heat resistance as raw material is more desired and the ratios of the *trans*-form to the *cis*-form are usually chosen from 100/0 to 60/40 depending on the requirement of the application [6]. It can be seen from Table 2 that the *trans*/*cis* ratio 36/64 using 2.8 wt% Rh/SBA-15 could be increased to 70/30 using 5.6 wt% Rh/SBA-15 by simply increasing Rh content to meet the requirement of the application. It can also be seen from Table 2 that almost all the *trans*/*cis* ratios obtained from Rh-Pt bimetallic catalysts were in the range required for application. Thus, these bimetallic catalysts containing relative cheaper Pt should be more attractive for industrial use.

The stability tests were performed as well in this study to examine the reusability of $Rh_{70}Pt_{30}$/SBA-15 for hydrogenation of TPA. After reaction, the solvent was removed by evaporation and DMSO-d_6 was used to dissolve the product. The catalyst was filtered and dried before the next run. As shown in Fig. 5, a complete conversion of TPA over $Rh_{70}Pt_{30}$/SBA-15 was achieved in the first cycle. After the fifth cycle, the specific activity of $Rh_{70}Pt_{30}$/SBA-15 prepared by CFD decreased 17.7% as compared with that in the first cycle and the conversion was still higher than 80% as shown in Fig. 5. Moreover, the ratios of the *trans*-form to the *cis*-form in all the cycles were higher than 60/40, satisfying the requirement for industrial application. These results verified that the bimetallic catalyst synthesized by CFD was stable for hydrogenation, which is required for the industrial application.

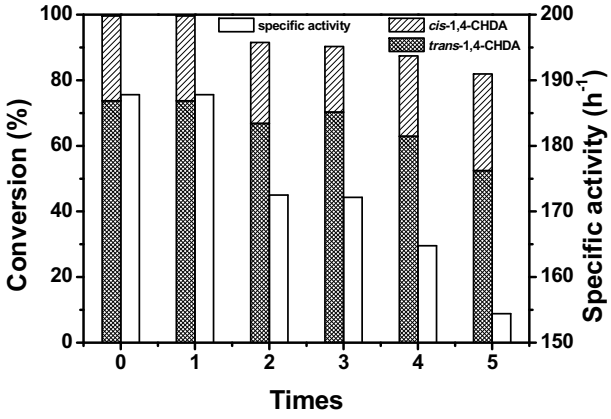

Fig. 5. Stability tests of $Rh_{70}Pt_{30}$/SBA-15 for hydrogenation of TPA. Reaction condition: 0.0250 g $Rh_{70}Pt_{30}$/SBA-15, 0.3 g TPA, 50 g water, 5 MPa H_2, 80 °C, and 4 h.

3.3. Hydrogenation of other aromatic compounds in water

The hydrogenation of other aromatic compounds, including bisphenol A (BPA), benzoic acid, isophthalic acid (IPA), and dimethyl phthalate (DMP) was investigated under the same mild reaction conditions (5 MPa of H_2 at 80 °C) over the prepared $Rh_{70}Pt_{30}$/SBA-15 bimetallic catalyst (Fig. 6) synthesized by CFD to demonstrate its wide applications. The detailed reaction conditions and results are presented in Table 3. It can be seen that a complete conversion of BPA could be achieved in 1 h, which was faster than the reaction time reported by Yen et al. [15] under similar reaction conditions. This higher catalytic activity can be attributed to the synergistic effect of Rh and Pt in the bimetallic catalyst. Thus, the bimetallic catalysts synthesized by CFD were found to exhibit a higher activity than the reported values in the literature. The $Rh_{70}Pt_{30}$/SBA-15 bimetallic catalyst with uniform particle dispersion offered more activate sites for the adsorption of benzene rings during hydrogenation. In addition, it was observed that complete conversion of benzoic acid, IPA, and DMP could be achieved under mild conditions in a relatively short reaction time. Based on these results, it was confirmed that the prepared bimetallic catalyst was highly active for the hydrogenation of the aromatic compounds

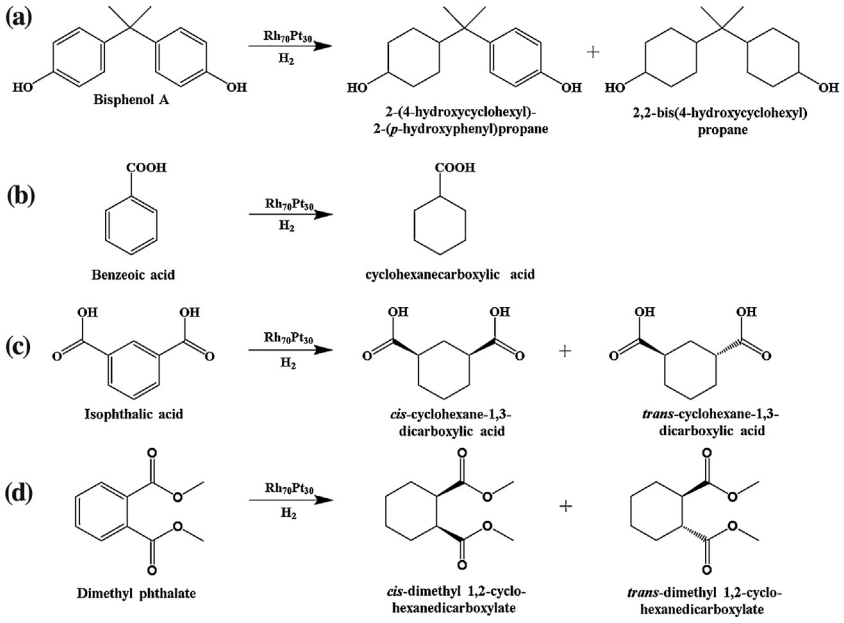

Fig. 6. The scheme of hydrogenation of BPA (a), hydrogenation of benzoic acid (b), hydrogenation of IPA (c), and hydrogenation of DMP (d).

Table 3
The hydrogenation of BPA, benzoic acid, IPA and DMP in water over the $Rh_{70}Pt_{30}$/SBA-15 bimetallic catalyst.

Reactant	Amount of reactant (g)	Reaction time (h)	Conversion (%)[a]	Specific activity (h^{-1})
BPA	0.5	0.5	82.5	1769
BPA	0.5	1	100	1828
Benzoic acid	0.5	0.5	100	3420
Benzoic acid	1	0.5	85.8	5868
IPA	0.5	4	100	628
DMP	5	3	87.3	3129
DMP	5	4	100	2688

[a] Reaction condition: $Rh_{70}Pt_{30}$/SBA-15 bimetallic catalyst synthesized by CFD (the theoretical metal loading was 5.6 wt%), 0.0250 g; water, 50 g; stir, 1000 rpm; H_2, 5 MPa; temperature, 80 °C.

containing benzene rings. Thus, this highly active bimetallic catalyst synthesized by CFD is expected to be applicable to the catalytic hydrogenation of benzene rings for most of the aromatic compounds.

4. Conclusions

In this study, we successfully synthesized an effective $Rh_{70}Pt_{30}$/SBA-15 bimetallic catalyst by CFD. The prepared bimetallic catalyst was found to be more active in the hydrogenation of TPA in water under mild conditions, despite the poor solubility of TPA in water. The XRD and TEM results confirmed that the average size of the $Rh_{70}Pt_{30}$ nanoparticles was ~6.1 nm and the SBA-15 support could retain its hexagonal mesoporous structure after depressurization in CFD. The TPA conversion was found to be 74.3% using the $Rh_{70}Pt_{30}$/SBA-15 bimetallic catalyst at 80 °C and 5 MPa of H_2 in a 2-h reaction, which was significantly higher than its monometallic counterparts under the same reaction conditions. Moreover, the introduction of a relatively cheaper noble metal (Pt) into the Rh catalyst as the main active species could reduce the cost. In addition, a complete conversion of TPA in water using the $Rh_{70}Pt_{30}$/SBA-15 bimetallic catalyst could be achieved at 80 °C within only 4 h, which not only could reduce the energy consumption and reaction time but also would avoid the hazardous waste treatment. This bimetallic catalyst was also found to be suitable for the hydrogenation of industrial aromatic compounds that have poor solubility in water such as BPA, benzoic acid, IPA and DMP. Moreover, a complete conversion of these compounds could be achieved using the bimetallic catalyst at 80 °C in a relatively short reaction time. The proposed reaction pathway can meet the requirements of green chemistry for sustainable development because of the use of green solvents in both the catalyst preparation and hydrogenation reactions.

Acknowledgement

The authors would like to acknowledge the financial support of the National Science Council, Republic of China (Taiwan), Grant (NSC 101-2221-E-007-118-MY3).

References

[1] Y. Tateno, C. Sano, K. Tanaka, M. Magara, N. Okamoto, K. Kato, Process for preparing 1,4-cyclohexandicarboxylic acid, US Patent 5430184 A, 1995.
[2] K. Endou, H. Nakamura, S. Tanaka, Process for producing *trans*-1,4-cyclohexanedicarboxylic acid, US Patent 7420086 B2, 2008.
[3] S. Hirayama, Y. Ishimura, K. Marumo, M. Miura, H. Monzen, K. Morikawa, T. Naito, T. Nozawa, Y. Suyama, Process for hydrogenating an aromatic ring containing compound using a ruthenium Raney catalyst, EP Patent 0724908 B1, 2002.
[4] H. Machida, K. Kedo, F. Zaima, Process for producing a hydrogenation product of an aromatic carboxylic acid, US Patent 20020115884 A1, 2002.
[5] C.E. Sumner, B.L.R. Gustafson, Hydrogenation of phthalic acids, CN Patent 1229322C, 2005.
[6] T. Tanaka, A. Kasai, Polyester resin, polyester resin composition, and sheet, film and hollow molded container obtained therefrom, US Patent 7048978 B2, 2006.
[7] S.L. Cook, G. Irick, C.S. Moorehouse, Process for preparation of cyclohexanedicarboxylic acid, US Patent 5118841 A, 1992.
[8] N. Han, L. Zhu, L. Wang, R. Fu, Sep. Purif. Technol. 16 (1999) 175–180.
[9] C.E. Sumner, B.L.R. Gustafson, Hydrogenation of phthalic acids to cyclohexanedicarboxylic acid, US Patent 6291706 B1, 2001.
[10] A. Kayou, Y. Nanba, Method for hydrogenation of terephthalic acid, JP Patent 2002145824, 2002.
[11] Z.Q. Zhu, Z.H. Lv, C.S. Sun, J.M. Xie, Method for producing 1,4-cyclohexane diformate by hydrogenation on benzene ring of terephthalic acid, CN Patent 1915958A, 2007.
[12] Q.Q. Xu, Y.L. Ma, X. Gang, J.Z. Yin, A.Q. Wang, J.J. Gao, J. Supercrit. Fluids 92 (2014) 100–106.
[13] Q.Q. Xu, Y.Q. Wang, A.Q. Wang, J.Z. Yin, L. Yu, Nanotechnology 23 (2012).
[14] C.H. Yen, H.W. Lin, D.P. The, C.S. Tan, J. Nanosci. Nanotechnol. 11 (2011) 2465–2469.
[15] C.H. Yen, H.W. Lin, C.S. Tan, Catal. Today 174 (2011) 121–126.
[16] H.J. Chen, H.W. Liu, W. Liao, H.B. Pan, C.M. Wai, K.H. Chiu, J.F. Jen, Appl. Catal. B 111–112 (2012) 402–408.
[17] R.P. Marin, S.A. Kondrat, R.K. Pinnell, T.E. Davies, S. Golunski, J.K. Bartley, G.J. Hutchings, S.H. Taylor, Appl. Catal. B 140–141 (2013) 671–679.
[18] C.M. Piqueras, V. Puccia, D.A. Vega, M.A. Volpe, Appl. Catal. B 185 (2016) 265–271.
[19] R.A. Lucky, P.A. Charpentier, Appl. Catal. B 96 (2010) 516–523.
[20] N. Farhangi, R.R. Chowdhury, Y. Medina-Gonzalez, M.B. Ray, P.A. Charpentier, Appl. Catal. B 110 (2011) 25–32.
[21] Q.Q. Xu, C.J. Zhang, X.Z. Zhang, J.Z. Yin, Y. Liu, J. Supercrit. Fluids 62 (2012) 184–189.
[22] Y. Zhao, J. Zhang, J. Song, J. Li, J. Liu, T. Wu, P. Zhang, B. Han, Green Chem. 13 (2011) 2078–2082.
[23] I. Nakamula, Y. Yamanoi, T. Imaoka, K. Yamamoto, H. Nishihara, Angew. Chem. Int. Ed. 123 (2011) 5952–5955.
[24] Y.H. Shih, M.Y. Chen, Y.F. Su, Appl. Catal. B 105 (2011) 24–29.
[25] F. Mauriello, H. Ariga, M.G. Musolino, R. Pietropaolo, S. Takakusagi, K. Asakura, Appl. Catal. B 166–167 (2015) 121–131.
[26] S. Cai, H. Duan, H. Rong, D. Wang, L. Li, W. He, Y. Li, ACS Catal. 3 (2013) 608–612.
[27] P. Benito, V. Dal Santo, V. De Grandi, M. Marelli, G. Fornasari, R. Psaro, A. Vaccari, Appl. Catal. B 179 (2015) 150–159.
[28] N. Seshu Babu, N. Lingaiah, P.S. Sai Prasad, Appl. Catal. B 111–112 (2012) 309–316.
[29] H.B. Pan, C.M. Wai, New J. Chem. 35 (2011) 1649–1660.
[30] P.L. Dhepe, A. Fukuoka, M. Ichikawa, Phys. Chem. Chem. Phys. 5 (2003) 5565–5573.
[31] R. Büchel, S.E. Pratsinis, A. Baiker, Appl. Catal. B 113–114 (2012) 160–171.
[32] S. Lim, C. Wang, Y. Yang, D. Ciuparu, L. Pfefferle, G.L. Haller, Catal. Today 123 (2007) 122–132.
[33] N.H.H. Abu Bakar, M.M. Bettahar, M. Abu Bakar, S. Monteverdi, J. Ismail, J. Mol. Catal. A Chem. 333 (2010) 11–19.
[34] B. Pawelec, V. La Parola, R. Navarro, S. Murcia-Mascaros, J. Fierro, Carbon 44 (2006) 84–98.
[35] D. Zhao, J. Feng, Q. Huo, N. Melosh, G.H. Fredrickson, B.F. Chmelka, G.D. Stucky, Science 279 (1998) 548–552.
[36] C.H. Huang, W. Klinthong, C.S. Tan, J. Supercrit. Fluids 77 (2013) 117–126.
[37] H. Rashidezadeh, B. Guo, J. Am. Soc. Mass Spectrom. 9 (1998) 724–730.
[38] C. Wang, H. Daimon, T. Onodera, T. Koda, S. Sun, Angew. Chem. Int. Ed. 47 (2008) 3588–3591.
[39] Q. Yuan, Z. Zhou, J. Zhuang, X. Wang, Chem. Commun. 46 (2010) 1491–1493.
[40] M. Ojeda, S. Rojas, M. Boutonnet, F.J. Pérez-Alonso, F. Javier Garcíía-Garcíía, J.L.G. Fierro, Appl. Catal. A 274 (2004) 33–41.
[41] K. Shimizu, J.S. Wang, I.F. Cheng, C.M. Wai, Energy Fuels 23 (2009) 1662–1667.
[42] H.J. Kim, S.M. Choi, S.H. Nam, M.H. Seo, W.B. Kim, Appl. Catal. A 352 (2009) 145–151.
[43] S. Yoda, Y. Mizuno, T. Furuya, Y. Takebayashi, K. Otake, T. Tsuji, T. Hiaki, J. Supercrit. Fluids 44 (2008) 139–147.

[44] T. Yuan, H. Gong, K. Kailasam, Y. Zhao, A. Thomas, J. Zhu, J. Catal. 326 (2015) 38–42.
[45] Y. Zhu, F. Zaera, Catal. Sci. Technol. 4 (2014) 955–962.
[46] B.V. Crist, Handbook of Monochromatic XPS Spectra: The Elements and Native Oxides, Wiley, 2000.
[47] J. Liu, Y. Li, J. Miao, Y.J. Ding, Chem. J. Chin. Univ. 37 (2016) 114–120.
[48] R.J. Isaifan, S. Ntais, E.A. Baranova, Appl. Catal. A 464–465 (2013) 87–94.
[49] R.N. Butler, A.G. Coyne, Chem. Rev. 110 (2010) 6302–6337.
[50] J. Greeley, M. Mavrikakis, Nat. Mater. 3 (2004) 810–815.
[51] J. Greeley, M. Mavrikakis, Catal. Today 111 (2006) 52–58.
[52] C.H. Yen, H.H. Wei, H.W. Lin, C.S. Tan, Appl. Organomet. Chem. 26 (2012) 736–742.
[53] J.L. Bills, A.C. Mckinnis, Separation of isophthalic and terephthalic acids, US Patent 2741633, 1956.
[54] S. Minakata, M. Komatsu, Chem. Rev. 109 (2009) 711–724.